



Lawrence Berkeley Laboratory

UNIVERSITY OF CALIFORNIA

Materials & Molecular Research Division

APR 14 1981
LIBRARY
DOCUMENTS

Submitted to Metallurgical Transactions

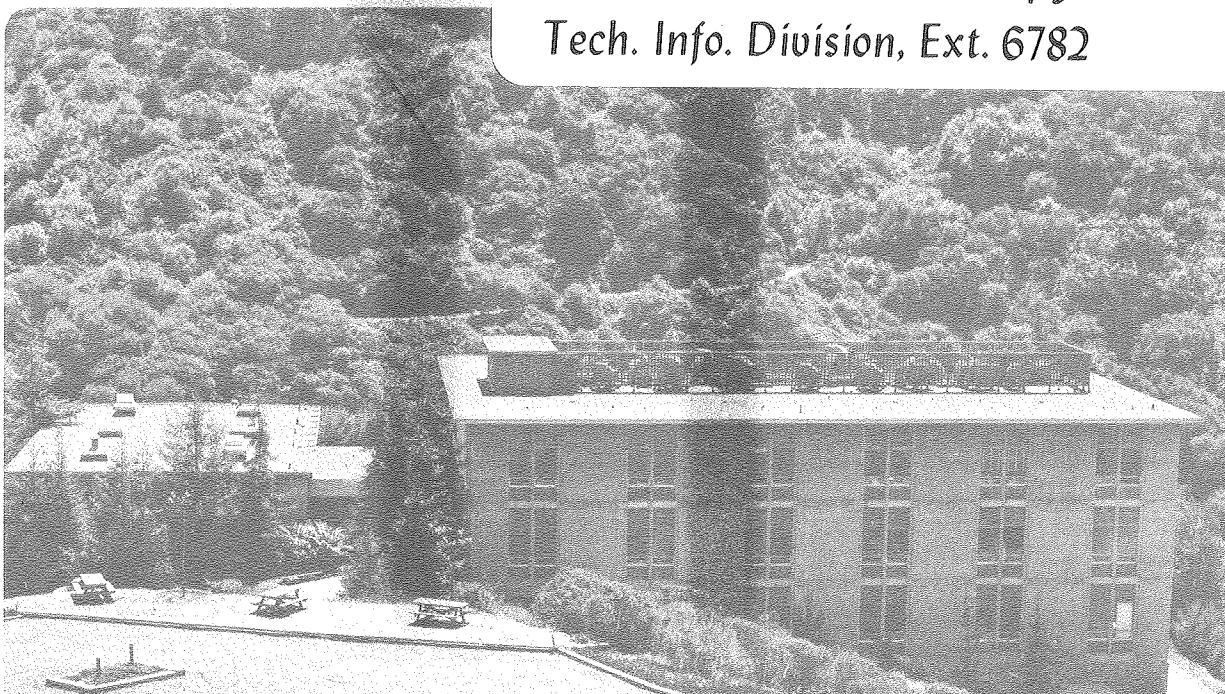
THE As-QUENCHED MICROSTRUCTURE AND TEMPERING
BEHAVIOR OF RAPIDLY SOLIDIFIED TUNGSTEN STEELS

J.J. Rayment and B. Cantor

April 1981

TWO-WEEK LOAN COPY

*This is a Library Circulating Copy
which may be borrowed for two weeks.
For a personal retention copy, call
Tech. Info. Division, Ext. 6782*



LBL-12121
c.2

DISCLAIMER

This document was prepared as an account of work sponsored by the United States Government. While this document is believed to contain correct information, neither the United States Government nor any agency thereof, nor the Regents of the University of California, nor any of their employees, makes any warranty, express or implied, or assumes any legal responsibility for the accuracy, completeness, or usefulness of any information, apparatus, product, or process disclosed, or represents that its use would not infringe privately owned rights. Reference herein to any specific commercial product, process, or service by its trade name, trademark, manufacturer, or otherwise, does not necessarily constitute or imply its endorsement, recommendation, or favoring by the United States Government or any agency thereof, or the Regents of the University of California. The views and opinions of authors expressed herein do not necessarily state or reflect those of the United States Government or any agency thereof or the Regents of the University of California.

The As-Quenched Microstructure and Tempering Behavior
of Rapidly Solidified Tungsten Steels

by

J. J. Rayment*

Materials and Molecular Research Division

Lawrence Berkeley Laboratory

University of California

Berkeley, California 94720

and

B. Cantor*

Department of Metallurgy and Science of Materials

University of Oxford

Oxford, England

* Formerly at School of Engineering and Applied Sciences, University of
Sussex, Falmer, Brighton, Sussex BN1 9QT, England

ABSTRACT

Transmission electron microscopy, and microhardness testing were used to examine the as-quenched structure and mechanical properties of a series of rapidly solidified (R.S.) iron-tungsten-carbon-alloys ranging from 6 to 23 percent tungsten with a constant W:C atomic ratio of 2:1, and T1 high speed tool steel. The R.S. iron-tungsten-carbon alloys were found to exhibit a significant change in microstructure and hardness as the tungsten and carbon content was increased. The change in morphology was from lath martensite in the lower tungsten alloys to a solidification structure of δ -ferrite cells surrounded by austenite and M_6C carbide, in the higher tungsten alloys. A model is proposed to explain the morphological change. In addition, the tempering behaviors of R.S. Fe-6.3wt%W-0.21wt%C, Fe-23wt%W-0.75wt%C and T1 high speed tool steel were examined and compared to those observed for the conventional solution-treated and quenched alloys.

A discussion is also included on the microstructural dependence upon cooling rate of R.S. high speed tool steels.

INTRODUCTION

Rapid solidification (R.S.), or as it is sometimes called, splat-quenching, has been a field of vigorous research activity in recent years, particularly in connection with metallic glasses. Lately, the R.S. of crystalline alloys has attracted increasing attention, especially in the case of iron-base alloys. The well known beneficial effects of R.S., namely refinement of grain size, homogenization of microstructure and extension of solid solubility, lend themselves well to typical microstructural problems found in conventional steels, such as an inhomogeneous microstructure with a coarse dispersion of carbides.

The present work described an investigation by transmission electron microscopy (TEM) and microhardness testing into the effects of R.S. upon a series of six iron-tungsten-carbon alloys and a tungsten-based commercial high speed steel, AISI T1. The three main reasons for investigating the ternary Fe-W-C alloys as well as T1 were as follows.

- 1) T1 is essentially an iron-tungsten-carbon alloy with additions of vanadium to prevent grain growth during solution treatment, and chromium to provide hardenability in the martensite, on quenching. These two additions would appear to have no obvious function in a rapidly solidified steel where there is no solid-state solution treatment and where martensite is often suppressed during the rapid quenching.
- 2) Phase transformations in high speed steels are complex under equilibrium conditions and have been shown to be further complicated when metastable, rapid quenching effects are taken into account.¹ It was hoped that the iron-tungsten-carbon alloys would present similar, but less complex microstructures and mechanical properties for interpretation.
- 3) The isothermal tempering behavior of solution-treated and brine-quenched Fe-6.3wt%W-0.21wt%C has been studied extensively.² R.S. of

this alloy would almost certainly result in a finer microstructure, and this might be expected to alter the isothermal tempering characteristics.

The iron-tungsten-carbon alloys ranged from 6.3wt% to 23wt% tungsten, with a constant tungsten:carbon atomic ratio of 2:1 (see Table 1). The Fe-23wt%W-0.75wt%C alloy was chosen to represent a simplified T1 steel, the carbon content being the same in both alloys, while the vanadium and chromium in T1 is replaced by additional tungsten in the ternary alloy. At the other end of the range of ternary alloys was the Fe-6.3wt%W-0.21wt%C alloy previously examined in the solid state.² The other four alloys were chosen to span the range between the two alloys mentioned above.

The effect of R.S. upon the microstructure and hardness of these ternary alloys as a function of composition was investigated and the relative isothermal tempering behaviors of R.S. and solid-state quenched Fe-6.3wt%W-0.21wt%C were compared. A preliminary investigation was also made of the relative isochronal tempering behaviors of R.S. and solid-state quenched Fe-23wt%W-0.75wt%C and T1 tool steel.

EXPERIMENTAL PROCEDURE

Commercial grade T1 high speed tool steel was obtained in the form of 13mm diameter rod. The other alloys, shown in Table 1, were prepared from >99.99% pure iron, tungsten and carbon by induction melting in recrystallized alumina crucibles under a dynamic argon atmosphere. The as-cast alloys were homogenized for 100 hours at 1130°C and specimens were taken from the homogenized alloys for rapid solidification. R.S. was achieved by means of a two-piston apparatus described previously.³ Individual specimens of ~0.7 gram mass were levitation melted in an argon atmosphere and then allowed to fall under gravity until

quenched between two pistons accelerated magnetically. The R.S. foils were generally 70-120 μ m in thickness and approximately 30mm in diameter. The effective cooling rate has been measured as $\sim 10^7$ Ks $^{-1}$ at the melting point, falling to $\sim 10^5$ Ks $^{-1}$ at 700°C.⁴

In order to compare the structural and mechanical properties of the R.S. alloys with solution treated and solid-state quenched alloys, specimens of the latter were obtained by cold rolling the homogenized alloys ~ 50 percent and then solution treating at 1150°C for 50 hours, followed by a brine quench. All heat treatments were carried out either in sealed silica capsules which had been evacuated and then flushed through with argon, or under a dynamic argon atmosphere. Microhardness testing was carried out using a Leitz microhardness tester with a Vickers diamond indenter. R.S. and solid-state quenched specimens were tested with 50 gram and 200 gram loads respectively. Thin foils were prepared for TEM by a jet polishing technique using a solution of 20 percent perchloric acid in methanol at $\sim -15^\circ$ C. A JEM 100C (120kV) microscope was used for the electron microscopy.

RESULTS

The As-Quenched State

In R.S. FeWC1-3, that is alloys containing up to 13wt% tungsten (see Table 1), the typical as-quenched microstructure was lath martensite, as seen in Fig. 1. The dimensions of the martensite laths in the three alloys varied only slightly and were of the order of 0.1 - 0.3 μ m in width and 1 - 3.0 μ m in length.

In R.S. FeWC4 alloy (16.5wt% tungsten), two types of microstructure were seen. In a few areas, a martensitic lath structure, similar to that seen in the lower tungsten alloys was present, but in all other

areas examined, a cellular, solidification structure was observed. An example of this cellular microstructure can be seen in Fig. 2. The microstructure was found to consist of δ -ferrite cells, $\sim 0.6 - 1.0\mu\text{m}$ in diameter, surrounded by austenitic cell boundaries $\sim 0.05 - 0.1\mu\text{m}$ thick. Fig. 2d is a selected area diffraction pattern (SAD) taken from the area shown in Fig. 2a. Using $(110)_{\alpha}$ and $(111)_{\gamma}$ reflections for centered dark field microscopy (CDF) it was possible to illuminate areas within a cell and cell boundary respectively (Figs. 2b-c).

In R.S. FeWC5-6 (20 and 23wt% tungsten) only the cellular microstructure was observed, with δ -ferrite cells, $0.3 - 1.0\mu\text{m}$ in diameter. In this case, however, the cell boundaries were found to contain not only austenite but also M_6C carbide. Figs. 3 and 4 show the cellular microstructure of the higher tungsten alloys. Selected area diffraction of the area shown in Fig. 4a revealed $[001]_{\gamma}$ and $[012]_{M_6C}$ zones with the orientation relationship

$$(110)_{\gamma} \parallel (100)_{M_6C}$$

$$(010)_{\gamma} \parallel (\bar{2}2\bar{1})_{M_6C}$$

Using a $(\bar{2}4\bar{2})_{M_6C}$ reflection, the CDF image shown in Fig. 4b was obtained. The carbide can clearly be seen to exist in the cell boundaries. In general, there did not appear to be a unique relationship between the austenite and M_6C carbide in the R.S. alloys. Indeed, many different orientation relationships were observed. Figure 5 shows the microhardness of R.S. and solid-state quenched Fe-W-C alloys as a function of tungsten content. All the solid-state quenched Fe-W-C alloys had microhardness values in the range $750-800\text{kgmm}^{-2}$. R.S. FeWC1 and 2 (6.3 and 9.5wt% tungsten) had microhardness values of

$\sim 700 \text{kgmm}^{-2}$, not very different from the solid-state quenched alloys. However, in FeWC4-6 (16.0 - 23.0wt% tungsten), the as-quenched hardness was much greater, $\sim 1050 \text{kgmm}^{-2}$.

As with FeWC5 and 6 (20 and 23wt%W) the as-quenched microstructure of R.S. T1 tool steel was found to consist of δ -ferrite cells surrounded by cell boundaries containing austenite and M_6C carbide. The cell dimensions were similar to those observed in R.S. FeWC5 and 6 alloys, and an example of the cellular microstructure is shown in Fig. 6. The hardness of R.S. T1 tool steel was 615kgmm^{-2} , in comparison to a hardness of 800kgmm^{-2} found in the commercial alloy quenched from the solid-state.⁵

The Tempering of Fe-6.3wt%W - 0.21wt%C

Fig. 7 shows the effect of isothermal tempering at 600°C on the microhardness of both R.S. and solid-state quenched FeWC1 (6.3wt%W). The tempering behavior of R.S. and solid-state quenched specimens was almost identical. In each case the as-quenched hardness of 700-800 kgmm^{-2} fell abruptly to 450-470 kgmm^{-2} after 1 hour at 600°C . This drop in hardness was followed by a small secondary hardening peak, with a peak hardness of 475-500 kgmm^{-2} after 2-3 hours, and then eventual overaging at times greater than 5 hours.

Specimens of R.S. FeWC1 (6.3wt%W) tempered at 600°C for 40 minutes, 10 hours and 50 hours were chosen for examination by TEM. These three specimens were picked to represent the initial softening, secondary hardening and overaging periods respectively. Because of difficulty found in obtaining a good TEM foil, truly representative of the secondary hardening stage, it was necessary to examine a specimen past the hardening peak, i.e. tempered at 600°C for 10 hours. However,

it was possible to establish, by TEM, that the structure, although coarser, was essentially the same. Transmission electron microscopy of R.S. FeWC1, tempered at 600°C for 40 minutes showed that the initial lath martensite structure was retained, but within the laths there was a Widmanstätten array of precipitates identified as cementite (Fe_3C), see Fig. 8. The cementite exhibited the Bagaryatski orientation relationship with the tempered martensite in agreement with the results obtained by Davenport,² namely,

$$\{110\}_\alpha \parallel (100)_{\text{Fe}_3\text{C}}$$

$$\langle 110 \rangle_\alpha \parallel [\bar{0}1\bar{0}]_{\text{Fe}_3\text{C}}$$

After tempering at 600°C for 10 hours, specimens of R.S. FeWC1 were found to contain a fine-scale precipitation on interlath and prior austenite grain boundaries and to a lesser extent, within the laths. Those precipitates which could be identified were W_2C carbides and the orientation relationship between W_2C and the tempered martensite was found to be consistent with that observed by Dyson et al.⁶ for Mo_2C in ferrite, namely

$$(110)_\alpha \parallel (00.1)_{\text{W}_2\text{C}}$$

$$[100]_\alpha \parallel [2\bar{1}.0]_{\text{W}_2\text{C}}$$

Whether there was still any cementite present could not be positively verified by either bright-field imaging or by selected area diffraction. A specimen of the tempered alloy was therefore further examined by a combination of scanning-transmission electron microscopy (STEM),

scanning secondary electron microscopy (SEM) and X-ray analysis by energy dispersive spectroscopy (EDS) in a JEM 100C TEMSCAN microscope. The SEM and STEM micrographs of one of the regions examined are shown in Fig. 9. The areas chosen for element microanalysis were (i) individual carbide particles visible in both SEM and STEM, points 1 - 7, and (ii) areas within the matrix that appeared to be free of any carbides, points 8 and 9. Table II lists the $W_{M\alpha}/Fe_{K\alpha}$ ratios for the individual points. These ratios show the existence of two types of carbide; one with a significant tungsten content as found at point 1, the other with little or no tungsten content at all, as found at point 4. The matrix was found to contain very little tungsten. The nature of elements present in tool steel carbides is relatively well known.⁵ In M_3C carbide, the metallic element is predominantly iron and the carbide can dissolve only a little tungsten, whereas M_2C is a tungsten-rich carbide. From this evidence, it is likely that the tungsten-rich carbide was indeed W_2C , and the carbide containing little or no tungsten was undissolved Fe_3C . There appeared to be no difference in morphology between the two types of carbide, and the relatively coarse cementite was found only at interlath boundaries, alongside W_2C precipitates.

After tempering at 600°C for 50 hours, R.S. FeWCl contained blocky precipitates along interlath and prior austenite boundaries, and to a lesser extent, precipitates within the tempered laths. The blocky precipitates were identified as M_6C carbides and the precipitates within the laths were undissolved W_2C carbides. Electron diffraction patterns of M_6C and tempered martensite were consistent with either a Kurdjumov-Sachs relationship

$$(011)_{\alpha} \parallel (\bar{1}\bar{1}\bar{1})_{M_6C}$$

$$[\bar{1}\bar{1}\bar{1}]_{\alpha} \parallel [011]_{M_6C}$$

or with a Nishiyama-Wasserman relationship

$$(011)_{\alpha} \parallel (\bar{1}\bar{1}\bar{1})_{M_6C}$$

$$[01\bar{1}]_{\alpha} \parallel [112]_{M_6C}$$

The ambiguity is not surprising considering that the two relationships differ by only $5^{\circ}16'$.

The Tempering of Fe-23wt%W - 0.75wt%C and T1 High Speed Steel

Fig. 10 shows the effect of isochronal tempering on the micro-hardness of R.S. and solid-state quenched FeWC6 and T1 tool steel. The conventional solid-state quenched T1 tool steel, (commercial data, see Ref. 5), showed a softening at $\sim 300^{\circ}\text{C}$, followed by a secondary hardening peak of 950kmm^{-2} at $\sim 530^{\circ}\text{C}$. In R.S. T1, a large scatter in the hardness measurement at the lower temperatures made it difficult to determine if any softening had occurred. However, a large secondary hardening peak was observed at $\sim 650^{\circ}\text{C}$ with a peak hardness of $\sim 1050\text{kmm}^{-2}$. There was no obvious secondary hardening in the solid-state quenched FeWC6. The as-quenched hardness of $\sim 800\text{kmm}^{-2}$ dropped gradually to $\sim 650\text{kmm}^{-2}$ at 500°C and then further decreased to $\sim 400\text{kmm}^{-2}$ at 650°C . The curve for the R.S. alloy, on the other hand, showed an initial softening at 350°C , and then a secondary hardening of $\sim 1000\text{kmm}^{-2}$ at 600°C followed by overaging at higher temperatures.

The effect of tempering on the microstructure of R.S. FeWC6 and

T1 was not examined in full detail, but TEM studies showed that in FeWC6, cementite precipitation occurred at 300-500°C, followed by M_6C precipitation within the cells at 650°C. In addition a significant proportion of the austenite in the cell walls transformed to bcc-iron by 550-650°C, although it was not possible to identify positively the bcc phase, see Fig. 11. During the tempering of T1, there was little change in microstructure until 615°C, where fine M_2C needles were precipitated within the ferrite cells. This corresponded to the peak hardness. The precipitation of M_2C , as shown in Fig. 12, was much finer than the M_6C precipitation observed in the tempered FeWC6 alloy. The majority of the austenite was still present after tempering at 615°C.

DISCUSSION

The As-Quenched Structure

The as-quenched microstructure of R.S. FeWC1-3 is essentially fine-scale lath martensite. The martensitic nature of FeWC1 is not surprising, as it has been shown previously that solid-solution treatment of the same alloy is capable of taking all the carbides into solution, and producing a martensitic structure on quenching.² The R.S. microstructure, however, is 5-10 times finer than that obtained in the solid-state quenched alloy. The alloy systems Fe-4wt%Mo-0.2wt%C,⁷ Fe-2wt%V-0.2wt%C⁷ and Fe-9wt%Cr-0.2wt%C⁸ (all having a similar atomic composition to FeWC1) have also been shown to form a fully martensitic as-quenched structure after suitable solution treatments in the solid-state. In addition, one of these alloys, Fe-4%Mo-0.2%C, has been examined after rapid solidification by Sare⁹ using a gun technique which gave specimens of varying thickness. In thin, electron transparent

regions, Sare found δ -ferritic grains elongated in the plane of the foil but was not able to detect any martensite. In slower-cooled, thick regions, however, the structure was mainly finely-twinned martensite, with some retained high temperature ferrite. The estimated cooling rate for the gun rapid-quencher is $10^6 - 10^8 \text{ Ks}^{-1}$,¹⁰ in comparison to $10^5 - 10^7$ for the two-piston apparatus used in this investigation. Therefore, the fact that δ -ferrite is present in splat-quenched Fe-4wt%Mo-0.2wt%C and not in Fe-6.3wt%W-0.21wt%C is probably a consequence of the different rates of cooling. A more detailed discussion of the effect of cooling rate on microstructure is presented in the next section.

The microstructures of R.S. FeWC2 and 3 differ from those obtained for the solution-treated/brine-quenched alloys. In the former there is complete solid solubility, whereas the latter alloys have been shown previously to contain significant amounts of M_6C carbide with the carbide content increasing with alloy content.^{11,12} The primary effect of rapid solidification on iron-tungsten-carbon alloys containing up to 13wt% tungsten is, therefore, to produce a fine scale martensitic microstructure with complete solution of alloying elements.

The cellular microstructure observed in the higher tungsten, R.S. alloys (>13wt%W) is not observed in the corresponding solid-state quenched alloys where it has been previously shown that the only phases present are bcc-iron, identified by optical microscopy as martensite, and M_6C carbide.^{11,12} The as-quenched microstructure of R.S. T1 tool steel is also different from that observed in the conventionally treated alloy which has been found to be a severely cored structure of predominantly martensite with austenite, M_6C carbide and possibly a little retained δ -ferrite.⁵ The amount of carbide present in both solid-state

quenched FeWC4-6 and in T1 tool steel is significantly higher than that detected in the R.S. alloys. The non-martensitic cellular microstructure of R.S. FeWC4-6 and T1 is, therefore, very different from the structures seen in the solution-treated and quenched alloys.

The Effect of Cooling Rate on Rapidly Solidified High Speed Tool Steels

Several investigations into the rapid solidification of high-speed steels have shown different as-quenched microstructures. The results of these experiments are summarized in Table III. The differences in the structure of high speed tool steels obtained on rapid solidification can be explained as the result of different rates of cooling. The investigations by Arai and Komatsu^{13,14} and Niewiarowski and Matyja¹⁵ almost certainly used relatively low cooling rates. In the results obtained by Arai and Komatsu, the microstructure was primary γ and eutectic γ and carbide, with ferrite found only in a few cases, and in the results of Niewiarowski and Matyja, the bcc phase was not properly identified but from X-ray and hardness data it was probably either martensite or a mixture of martensite and δ -ferrite. In the investigations by Jama and Thursfield,¹⁶ Tuli et al.^{17,18} and Sare,¹ higher cooling rates were obtained, and the δ -ferrite phase was found in large quantities in the rapidly solidified material. Jama and Thursfield¹⁶ found δ -ferrite close to the foil surface, while in the work of Tuli et al.,^{17,18} the δ -ferrite existed as cells surrounded by regions of austenite, M_2C and $M_{23}C_6$ carbide. In the work by Sare,¹ δ -ferrite was found in unthinned regions (which were assumed to be the fastest cooled) in the form of elongated dendrites and also as dendrites with interdendritic carbide precipitation. Austenite was found only in the thicker regions which were presumably cooled more slowly.

It is obvious that the rate of cooling has a strong effect on the R.S. microstructure of high speed tool steels. As the rate of cooling is increased from conventional levels of 10^3Ks^{-1} , up to rates commonly obtained in rapidly solidification experiments, austenite ($\sim 10^5 \text{Ks}^{-1}$) and eventually δ -ferrite ($\sim 10^7 - 10^8 \text{Ks}^{-1}$) become increasingly stabilized. From the microstructural evidence obtained by electron microscopy and from the recently measured cooling rate of 10^7Ks^{-1} achieved by the two-piston, splat-quencher,⁴ it would appear that the present work lies between the experimental results of Tuli et al.^{17,18} and that of Sare,¹ on the scale of increasing cooling rate, and is in reasonably good agreement with the previous results.

In the present investigation, the as-quenched microstructure of R.S. T1 tool steel is similar to laser-glazed microstructures obtained by Tuli et al.^{17,18} but there seems to be a disagreement about the type of carbide present. With electron diffraction of extraction replicas, Tuli suggested that the carbides in the cell walls are predominantly M_2C with some M_{23}C_6 , whereas in the present investigation the carbide has been identified as M_6C . However, it is difficult to differentiate between M_{23}C_6 and M_6C because of the similarity in the electron diffraction patterns for these types of carbides; M_{23}C_6 has an fcc structure and M_6C has an fcc diamond structure, and the lattice parameters are 10.621\AA and 11.08\AA respectively. Although neither investigation has determined conclusively which of the carbides is present, M_6C is more likely, because it is the more common solidification carbide. It may appear that the present investigation is in disagreement with previously reported results in which the microstructures of R.S. tool steels were shown to be predominantly austenite.¹⁹ In the previous reports, however, the microstructure was determined by X-ray diffractometry of the

whole foil, whereas in the present investigation, the structure was determined by TEM from the central faster-cooled regions of the foil.

The Change in Morphology in Rapidly Solidified Iron-Tungsten-Carbon Alloys and T1 Tool Steel

The conventional solidification and cooling sequences of FeWC1-6 alloys and T1²⁰ tool steel are shown in Table IV. The solidification data for iron-tungsten-carbon alloys was obtained from binary sections of the ternary phase diagram constructed by Takeda²¹ in the 1930's. In all the alloys, the peritectic reaction rarely goes to completion, even at relatively slow rates of cooling, and the remaining melt either transforms to supersaturated austenite (in alloys FeWC1-2) or transforms eutectically to austenite and M_6C carbide (in alloys FeWC3-6). On further cooling the δ -ferrite decomposes to austenite which eventually transforms to martensite. The solidification carbide, M_6C forms at different stages of cooling, depending on the alloy composition. In FeWC1-2, M_6C precipitates from the supersaturated austenite, and in FeWC3-4, it precipitates eutectically from the melt. Only in FeWC5-6 does M_6C carbide form at the early stages of solidification, from the peritectic reaction.

R.S. iron-tungsten-carbon alloys show a dramatic change in structure at 13-16.5wt% tungsten. Below this tungsten content, the as-quenched structure is martensitic, but at higher tungsten content, the structure is cellular, δ -ferrite with austenite and M_6C carbide in the cell boundaries. In R.S. FeWC1-3 (≤ 13 wt% tungsten), the martensitic microstructure indicates that the solidification reactions undergone during quenching are those shown in Table IV. In these alloys, precipitation of M_6C carbide from the supersaturated austenite

is completely suppressed. In R.S. FeWC4 (16.5wt% tungsten) the cellular microstructure of δ -ferrite and austenite indicates that solidification proceeds only as far as the peritectic formation of austenite. The eutectic reaction and all subsequent solid-state transformations are suppressed. In R.S. FeWC5-6 (>16.5wt% tungsten) the solidification reactions are the same as shown for FeWC4, but with M_6C as well as austenite produced by the peritectic transformation. Because of the similarities between the R.S. microstructure and the phase diagrams of T1 tool steel and FeWC6 alloy, the solidification reactions under rapid solidification conditions are assumed to be the same.

Fig. 13 shows the equilibrium temperatures of (i) the $\delta \rightarrow \gamma$ transformation, (ii) the T_0 temperatures of the $\delta \rightarrow \gamma$ transformation and (iii) the start of the $\gamma \rightarrow \alpha$ transformation as a function of tungsten content in iron-tungsten-carbon alloys. The data was taken from the iron-tungsten-carbon binary sections by Takeda.²¹ It can be seen that increasing the tungsten (and carbon) content effectively decreases the region of austenite stability by a combination of (a) lowering the $\delta \rightarrow \gamma$ transformation temperature and (b) raising the $\gamma \rightarrow \alpha$ transformation temperature.

Although the $\delta \rightarrow \gamma$ transformation is usually a diffusional process, it is possible for this reaction to be diffusionless. From the temperature range of austenite stability, shown in Fig. 13, and from the estimated rate of cooling, it is possible to calculate the time available for a diffusional $\delta \rightarrow \gamma$ transformation to occur, before the ferrite phase becomes stable once more. With the time known, and the diffusivities estimated for tungsten and carbon in δ -ferrite, the probability of such a $\delta \rightarrow \gamma$ diffusional transformation can be determined. By using the equation²²

$$X = \sqrt{Dt}$$

where X is the diffusional distance, D the diffusion coefficient and t , the time, it was found that if only the diffusion of carbon is considered, then the diffusional transformation is unlikely because the diffusional distance ($\sim 0.35\mu\text{m}$) is smaller than the δ -ferrite cell size ($\sim 0.5 - 1.0\mu\text{m}$). This is true if it is assumed that the nucleation of austenite is difficult within the cell and that austenite is formed by the growth of existing austenite at the cell boundaries. Moreover, if the diffusion of tungsten is considered necessary as well, then the diffusional transformation is surely not possible; the diffusional distance in this case is $\sim 0.01\mu\text{m}$.

The as-quenched microstructure of the iron-tungsten-carbon alloys shows that in the alloys containing up to and including 13wt% tungsten, a $\delta \rightarrow \gamma$ transformation (and subsequent $\gamma \rightarrow \alpha'$ transformation) did occur. Therefore, it is likely that the $\delta \rightarrow \gamma$ transformation was diffusionless. However, in the R.S. iron-tungsten-carbon alloys containing more than 13wt% tungsten, the as-quenched microstructure indicates that only the peritectic $L + \delta \rightarrow \gamma(+M_6C)$ reaction has taken place with no subsequent diffusional or diffusionless $\delta \rightarrow \gamma$ transformation. Therefore, in R.S. FeWC4-6, the rate of cooling is too fast for any $\delta \rightarrow \gamma$ transformation to occur.

In the later stages of cooling, the R.S. FeWC1-3 alloys undergo a $\gamma \rightarrow \alpha'$ martensitic transformation. From the equation relating composition to M_s ,²²

$$M_s(^{\circ}\text{C}) = 561 - 474(^{\circ}\text{C}) - 33(\% \text{Mn}) - 17(\% \text{Ni}) \\ - 17(\% \text{Cr}) - 13(\% \text{W})$$

all three alloys have a M_s significantly above room temperature, even when taking into account the effect of small grain size on the M_s temperature, which has been shown to depress the M_s temperature by as much as 200°C in R.S. ferrous alloys.²³ The estimated values are well above room temperature. However, in the R.S. FeWC4-6 alloys, the austenite present is peritectic austenite, enriched by the segregation of tungsten and carbon during solidification. In this situation, it is not possible to estimate the composition of the austenite, but obviously the enrichment will serve to lower the M_s temperature. These alloys have a high alloy content and therefore low M_s temperatures (commercial T1 has an M_s of 220°C). With the high composition of austenite in addition to the M_s depression caused by the small grain size, it is not surprising that the austenite is stable at room temperature.

The As-Quenched Hardness

The hardness results of R.S. iron-tungsten-carbon alloys and T1 are, on the whole, difficult to explain, and it has not been possible to achieve a good interpretation.

The as-quenched hardness of R.S. iron-tungsten-carbon alloys shows a significant increase when the microstructure changes from martensite to cellular ferrite. In the martensitic alloys, the hardness is $\sim 700 - 750 \text{ kgmm}^{-2}$, while in the cellular ferritic alloys, the hardness is $1050 - 1100 \text{ kgmm}^{-2}$. This is surprising as ferrous martensites are generally hard alloys with high dislocation densities whereas ferrite is usually a relatively soft phase. There are four effects that might be considered possible causes of the high hardness of the ferritic alloys:

- (i) Autotempering may have occurred in the martensite during cooling. There was no evidence of this, however, in transmission

electron microscopy.

- (ii) A high hardness might be expected if the δ -ferrite cells were much smaller than the martensite plates. This, however, was not the case.
- (iii) The δ -ferrite may have contained a high dislocation density as a result of being squeezed between two fast-moving pistons. However, this would apply equally to the martensite and therefore cannot be the reason for the significant difference in hardness.
- (iv) Solid solution hardening would have increased with increasing tungsten content and may become a significant effect in the δ -ferritic alloys. This has not been confirmed, but is quite probable.

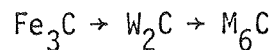
R.S. and solid-state quenched FeWCl (6.3wt% tungsten) have almost the same as-quenched hardness of approximately 750kgmm^{-2} . The as-quenched hardness of the same solid-state quenched alloy as studied by Davenport² was $\sim 500\text{kgmm}^{-2}$. It is possible that this difference is related to a difference in martensite lath dimensions. Recent work by Duflos and Cantor²⁴ on R.S. pure iron, has shown that a small martensite lath or plate size can lead to a very high hardness by a Hall-Petch effect. The martensite lath dimensions for the R.S. and solid-state quenched FeWCl alloy are typically $\sim 2\mu\text{m}$ in length and $\sim 0.2 - 0.5\mu\text{m}$ in width (R.S.) and $10 - 15\mu\text{m}$ in length and $\sim 1.0\mu\text{m}$ in width (solid-state quenched). This compares to the typical lath dimensions of $\sim 30\text{m}$ and 2.0m seen in Davenport's alloy.² It is difficult to explain why the R.S. and solid-state quenched hardnesses of FeWCl are so similar when the R.S. microstructure is five times finer. The difference between the hardness of the solid-state quenched alloys of

the present investigation and of Davenport's,² however, may be a direct consequence of a finer microstructure produced by a faster, more efficient brine quench.

The hardnesses of R.S. FeWC6 and T1 tool steel are $\sim 1050 \text{kgmm}^{-2}$ and $\sim 600 \text{kgmm}^{-2}$ respectively. There is no obvious reason for the difference, as the as-quenched microstructures are essentially the same and of similar dimensions. In addition, neither alloy appears to have undergone carbide precipitation during quenching.

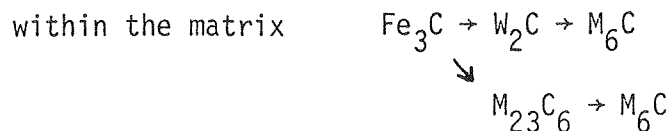
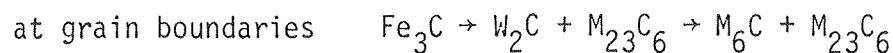
The Tempering of Rapidly Solidified Fe-6.3wt%W-0.21wt%C

The tempering sequence in R.S. Fe-6.3wt%W-0.21wt%C is as follows



The appearance of Fe_3C after 40 minutes at 600°C coincides with a drop in hardness from ~ 750 to $\sim 470 \text{kgmm}^{-2}$. After $2\frac{1}{2}$ hours at 600°C , precipitation of W_2C carbide has occurred, although some cementite has remained in the form of coarse particles on lath and grain boundaries; the hardness has risen and there is a secondary hardening peak, with a hardness of $\sim 500 \text{kgmm}^{-2}$. After 50 hours at 600°C , M_6C carbide precipitation is well established and produced a drop in hardness to $\sim 400 \text{kgmm}^{-2}$, although some W_2C carbide is still present.

In comparison a very similar tempering sequence for Fe-6.3wt%W-0.23wt%C solution treated and brine-quenched was found by Davenport² to be:



Davenport observed that the $\text{Fe}_3\text{C} \rightarrow \text{W}_2\text{C}$ reaction did not go to completion. Instead the unconsumed cementite transformed to M_{23}C_6 probably by nucleation on the cementite/ferrite interface. It may be that a similar precipitation occurs in R.S. and tempered FeWC1, but as mentioned previously, it is not easy to differentiate conclusively between M_6C and M_{23}C_6 carbides.

In addition to the tempering of R.S. FeWC1, the present investigation includes the tempering of solution treated and brine-quenched FeWC1. The solid-state quenched alloy displays a very similar tempering curve to that observed for the R.S. alloy, although with a hardness generally 20-30kgmm⁻² lower. It is, however, ~50kgmm⁻² higher than the tempering curve reported by Davenport.² The most likely reason for this difference is that the quench obtained in the present investigation is faster and produces a finer, harder microstructure (see last section).

The Tempering of Rapidly Solidified Fe-23wt%W-0.75wt%C and T1 High Speed Tool Steel

During the isochronal tempering of R.S. Fe-23wt%W-0.75wt%C M_6C carbide precipitates in the ferrite cells whereas during the tempering of R.S. T1, M_2C carbide precipitates. The difference in the type of carbide may possibly be due to the presence of vanadium and chromium in the high speed tool steel. It was observed that during the tempering of R.S. FeWC6, a significant amount of the austenite had transformed to bcc-iron at 550-650°C, whereas in the R.S. T1, the majority of austenite was retained. During tempering, the austenite present in the cell boundaries of FeWC6 may have transformed isothermally to ferrite and cementite, however, the presence of vanadium and chromium in T1 effectively retarded this transformation and only a small amount of austenite decomposed.

In R.S. FeWC6 and T1, the isochronal tempering curves show a hardening peak at higher temperatures and higher hardnesses than observed in the conventional solid-state quenched alloys. This effect is stronger in T1, where the shift in the hardness peak to higher hardness and temperature is greater than the equivalent shift in FeWC6. The increase in peak hardness for the R.S. alloys is presumably a consequence of the fine-scale of the precipitation. The higher hardness of T1 than that of FeWC₆ is almost certainly due to the different type of carbide formed during tempering and also because of the finer scale of precipitation in T1 than in FeWC₆. The higher peak temperatures of both R.S. alloys has been caused by a delay in the onset of M₂C precipitation, but what effect has produced this delay is not known.

CONCLUSIONS

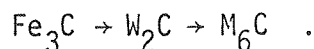
The following conclusions can be drawn from the investigation into the effect of rapid solidification on iron-tungsten-carbon alloys and T1 high speed steel.

- 1) Rapid solidification of iron-tungsten-carbon alloys containing less than or equal to 13wt% tungsten ($\leq 0.42\text{wt}\% \text{C}$) produces a fine martensitic lath microstructure.
- 2) Rapid solidification of iron-tungsten-carbon alloys containing 16.5wt% tungsten ($0.54\text{wt}\% \text{C}$) produces a microstructure mainly of δ -ferrite cells surrounded by austenite cell boundaries but with some small areas where there is a martensitic lath structure, similar to that seen in the lower tungsten alloys.
- 3) Rapid solidification of iron-tungsten-carbon alloys containing greater than 16.5wt% tungsten ($0.54\text{wt}\% \text{C}$) and up to 23wt% tungsten ($0.75\text{wt}\% \text{C}$) produces a solidification microstructure of δ -ferrite

- cells surrounded by cell boundaries of austenite and M_6C carbide.
- 4) The iron-tungsten-carbon alloys which are martensitic on rapid solidification have a hardness of $\sim 700 \text{kgmm}^{-2}$, whereas the alloys which are cellular ferritic on rapid solidification have a hardness of $\sim 1050 - 1100 \text{kgmm}^{-2}$. This is difficult to explain but may be a consequence of solid-solution strengthening.
 - 5) Rapid solidification of T1 high speed steel produces a solidification microstructure of δ -ferrite cells surrounded by cell boundaries of austenite and M_6C carbide. The structure is essentially the same as seen in the high tungsten ternary alloys ($>16.5\text{wt\% tungsten}$).
 - 6) The as-quenched microstructure of R.S. high speed steels is very dependent on the rate of cooling. At cooling rates of $\sim 10^8 \text{Ks}^{-1}$, the structure is almost entirely δ -ferrite. At slightly lower cooling rates of $\sim 10^6 - 10^7 \text{Ks}^{-1}$, as obtained in the present investigation, δ -ferrite cells are retained to room temperature but are surrounded by a region of austenite and carbide (either M_6C or M_2C). At even lower cooling rates ($\sim 10^5 \text{Ks}^{-1}$) almost no δ -ferrite is retained, and the microstructure is austenite with possibly some martensite. As the cooling rate reaches conventional levels (i.e. $\sim 10^3 \text{Ks}^{-1}$), the microstructure is predominantly martensitic with a little retained austenite, with large quantities of as-solidified carbide.
 - 7) There is a critical alloy content in iron-tungsten-carbon alloys, above which δ -ferrite is retained but below which the $\delta \rightarrow \gamma$ and subsequent $\gamma \rightarrow \alpha'$ transformations occur. It is probable that the diffusional $\delta \rightarrow \gamma$ transformation is too slow to occur in any of the R.S. alloys. Instead, in alloys containing less than

16.5wt% tungsten, it is likely that a diffusionless $\delta \rightarrow \gamma'$ transformation occurs. In R.S. alloys containing $\geq 16.5\text{wt}\%$ tungsten, however, the diffusionless $\delta \rightarrow \gamma$ transformation does not occur and δ -ferrite and the peritectic austenite and carbide are retained to room temperature.

- 8) The isothermal tempering behavior of R.S. Fe-6.3wt%W-0.21wt%C at 600°C is very similar to the alloy quenched from the solid-state with the following precipitation sequence



The precipitation of Fe_3C is accompanied by a drop in hardness from 750 - 470 kgmm^{-2} . The onset of secondary hardening with a peak hardness of $\sim 500 \text{kgmm}^{-2}$ corresponds to the precipitation of W_2C carbide. Overaging follows, and the formation of M_6C carbide produces a gradual drop in hardness.

- 9) During the isochronal tempering of R.S. Fe-23wt%W-0.75wt%C and T1 high speed tool steel, Fe_3C and M_6C precipitate in the former while M_2C precipitates in the latter. The presence of chromium and vanadium in R.S. T1 appears to modify the precipitation process compared to R.S. Fe-23wt%W-0.75wt%C.
- 10) The isochronal tempering curves for R.S. Fe-23wt%W-0.75wt%C and T1 show a secondary hardening peak at higher temperatures and hardnesses than observed for the conventional solution-treated and quenched alloys. The higher peak hardnesses of the R.S. alloys are probably the result of a much finer scale of precipitation.

ACKNOWLEDGEMENTS

The authors are grateful to Professor R. W. Cahn for provision of laboratory facilities and to Drs. R. D. Doherty, J. Perkins and S. Banerjee for fruitful discussion. We would also like to thank JEOL UK Ltd. for the use of the JEOL 100C TEMSCAN Microscope. One of us (JRR) would like to acknowledge and thank the Science Research Council for the provision of a studentship and both authors would like to acknowledge the financial support of the U. S. Office of Naval Research (Grant number N-00014-78-G-0048). This work was also partially supported by the Director, Office of Energy Research, Office of Basic Energy Sciences, Materials Sciences Division of the U. S. Department of Energy under Contract No. W-7405-ENG-48.

REFERENCES

1. I. R. Sare and R. W. K. Honeycombe, *Metal Science J.*, 1979, vol. 13, pp. 269-279.
2. A. T. Davenport, Ph.D. Thesis, Sheffield UK, 1968.
3. R. W. Cahn, K. D. Khrishnanand, M. Laridjani, M. Greenholz and R. Hill, *Mat. Sci. & Eng.*, 1976, vol. 23, pp. 83-86.
4. F. Duflos, D.Phil. Thesis, Sussex, UK, 1980.
5. R. Wilson, "Metallurgy & Heat Treatment of Tool Steels", pp. 163-169 and 191, McGraw-Hill, London, 1975.
6. D. J. Dyson, S. R. Keown, D. Raynor and J. A. Whiteman, *Acta Met.*, 1966, vol. 14, p. 867.
7. D. Raynor, J. A. Whiteman and R. W. K. Honeycombe, *JISI*, 1966, vol. 204, p. 1114.
8. A. K. Seal and R. W. K. Honeycombe, *JISI*, 1958, vol. 188, p. 9.
9. I. R. Sare and R. W. K. Honeycombe, *J. of Mat. Sci.*, 1978, vol. 13, pp. 1991-2002.
10. J. V. Wood and I. R. Sare, "Proc. of 2nd International Conference on Rapidly Quenched Metals, vol. 1, pp. 87-94, MIT Press, 1976.
11. J. J. Rayment and B. Cantor, "Proc. of 3rd International Conference on Rapidly Quenched Metals", (ed. B. Cantor), vol. 1, pp. 85-93, The Metals Society, London, 1978.
12. J. J. Rayment, D.Phil. Thesis, Sussex, UK, 1979.
13. T. Arai and N. Komatsu, *Tetsu-to-Hagane*, 1972, vol. 58, p. 899.
14. T. Arai and N. Komatsu, *Tetsu-to-Hagane*, 1972, vol. 58, p. 1246.
15. J. Niewiarowski and H. Matyja, "Proc. of 3rd International Conference on Rapidly Quenched Metals", (ed. B. Cantor), vol. 1, pp. 193-196, The Metals Society, London, 1978.

16. S. A. B. Jama and G. Thursfield, Tube Investments Research Laboratories, Birmingham, U. K., Report No. 322, 1972.
17. M. Tuli, P. R. Strutt, H. Nowotny and B. H. Kear, Proc. of 2nd International Conference on Rapid Solidification Processing, pp. 112-115, Claitors, Baton Rouge, 1978.
18. P. R. Strutt, H. Nowotny and B. H. Kear, "Proc of 3rd International Conference on Rapidly Quenched Metals", vol. 1, pp. 171-175, The Metals Society, London, 1978.
19. J. J. Rayment and B. Cantor, Met. Sci. J. 1978, vol. 12, p. 156.
20. G. Hobson and D. S. Tyas, Metals & Materials, 1968, vol. 2, p. 144.
21. S. Takeda, Tech. Report of Tohoku Univ., 1931, vol. 10, p. 42.
22. P. G. Shewmon, "Transformations in Metals", p. 45 and 340, McGraw-Hill, New York, 1969.
23. Y. Inokuti and B. Cantor, Scripta Met., 1976, vol. 10, p. 655.
24. F. Duflos and B. Cantor, "Proc. of 3rd International Conference on Rapidly Quenched Metals", (ed. B. Cantor), vol. 1, pp. 110-118.

ALLOY	Weight % of alloying element (atomic %)				
	W	C	V	Cr	Fe
FEWC 1	6.3 (1.99)	0.21 (0.99)	-	-	balance
FEWC 2	9.5 (3.05)	0.32 (1.53)	-	-	"
FEWC 3	13.0 (4.27)	0.42 (2.14)	-	-	"
FEWC 4	16.5 (5.54)	0.54 (2.77)	-	-	"
FEWC 5	20.0 (6.80)	0.65 (3.43)	-	-	"
FEWC 6	23.0 (8.06)	0.75 (4.03)	-	-	"
T1	18.0	0.75	1.10	4.0	"

Table I: Chemical compositions of six ternary iron-tungsten-carbon alloys and commercial high speed tool steel T1.

AREA	1	2	3	4	5
Peak count	0.54	0.13	0.33	0.05	0.29
Integ. "	0.45	0.08	0.34	0.01	0.25
AREA	6	7	8	9	
Peak count	0.08	0.33	0.07	0.06	
Integ. "	0.05	0.31	0.03	0.04	

Table II. Peak counts and integrated counts of the $[W_{M\alpha}/Fe_{K\alpha}]$ ratio for rapidly solidified Fe-6.3wt%W-0.21wt%C, tempered at 600°C for 10 hours; Areas 1-7 are individual carbides and Areas 8-9 are within the matrix.

Authors	Tool Steel	i) Foil Thickness ii) Cooling Rate	Phases Present
Arai and Komatsu, refs. 13, 14	M2	i) 500 - 1500 μ m	i) primary γ , eutectic $\gamma + M_2C + MC$ ii) δ -ferrite, eutectic $\gamma + M_2C + MC$
Niewiarowski and Matyja, ref. 15	T1	i) 30 - 400 μ m	bcc-iron, γ and M_6C
Jama and Thursfield, ref. 16	M2 and T1	i) $\sim 100\mu$ m	δ -ferrite, γ (no carbide detected by optical microscopy)
Tuli <u>et al</u> , refs. 17, 18	T1	ii) $\sim 10^6 \text{Ks}^{-1}$	δ -ferrite, $\gamma + M_2C$
Rayment and Cantor, refs. 11, 12, 19	M2, M42 and T1	i) 70 - 120 μ m ii) $\sim 10^7 \text{Ks}^{-1}$	i) γ , bcc-iron, carbide--see refs. 11, 19 ii) δ -ferrite, $\gamma + M_6C$ --see ref. 12
Sare, ref. 1	M1	ii) $\sim 10^6 - 10^8 \text{Ks}^{-1}$	δ -ferrite, carbide (either M_2C , M_6C or $M_{23}C_6$)

Table III: The results of previous investigations into the effect of cooling rate on the rapidly solidified structures of high speed tool steels.

ALLOY	FeWC1	FeWC2	FeWC3	FeWC4	FeWC5	FeWC6	T1
Conventional	$L \rightarrow \delta$	$L \rightarrow \delta$	$L \rightarrow \delta$	$L \rightarrow \delta$	$L \rightarrow \delta$	$L \rightarrow \delta$	$L \rightarrow \delta$
Solidification	$L + \delta \rightarrow \gamma$	$L + \delta \rightarrow \gamma$	$L + \delta \rightarrow \gamma$	$L + \delta \rightarrow \gamma$	$L + \delta \rightarrow \gamma + M_6C$	$L + \delta \rightarrow \gamma + M_6C$	$L + \delta \rightarrow \gamma$
& Cooling	$\gamma_{sup} \rightarrow \gamma + M_6C$	$\gamma_{sup} \rightarrow \gamma + M_6C$	$L \rightarrow \gamma + M_6C$	$L \rightarrow \gamma + M_6C$	$\gamma \rightarrow \alpha$	$\gamma \rightarrow \alpha'$	$L \rightarrow \gamma + M_6C$
Sequences	$\gamma \rightarrow \alpha'$	$\gamma \rightarrow \alpha'$	$\gamma \rightarrow \alpha'$	$\gamma \rightarrow \alpha'$			$\delta \rightarrow \gamma + M_6C$ $\gamma \rightarrow \alpha'$
Rapid	$L \rightarrow \delta$	$L \rightarrow \delta$	$L \rightarrow \delta$	$L \rightarrow \delta$	$L \rightarrow \delta$	$L \rightarrow \delta$	$L \rightarrow \delta$
Solidification	$L + \delta \rightarrow \gamma$	$L + \delta \rightarrow \gamma$	$L + \delta \rightarrow \gamma$	$L + \delta \rightarrow \gamma$	$L + \delta \rightarrow \gamma + M_6C$	$L + \delta \rightarrow \gamma + M_6C$	$L + \delta \rightarrow \gamma + M_6C$
Sequence	$\delta \rightarrow \gamma$	$\delta \rightarrow \gamma$	$\delta \rightarrow \gamma$				
	$\gamma \rightarrow \alpha'$	$\gamma \rightarrow \alpha'$	$\gamma \rightarrow \alpha'$				

Table IV: The conventional solidification and cooling sequences and the rapid solidification and cooling sequences for the six iron-tungsten-carbon alloys and T1 highspeed tool steel.

- Fig. 1. The martensitic lath microstructure of rapidly solidified FeWC1-3 alloys.
- Fig. 2a. The microstructure of rapidly solidified FeWC4 alloy showing δ -ferrite cells surrounded by regions of austenite.
- Fig. 2b. Area shown in Fig. 2a, viewed in dark field using a $(110)_{\alpha}$ reflection.
- Fig. 2c. Area shown in Fig. 2a, viewed in dark field using a $(111)_{\gamma}$ reflection.
- Fig. 2d. Selected area diffraction pattern of area shown in Fig. 2a.
- Fig. 3. The microstructure of rapidly solidified FeWC6 alloy, showing δ -ferrite cells surrounded by regions of austenite and M_6C carbide.
- Fig. 4a. The microstructure of rapidly solidified FeWC6 alloy
- Fig. 4b. Area shown in Fig. 4a, viewed in dark field using a $(\bar{2}4\bar{2})_{M_6C}$ reflection.
- Fig. 4c. Selected area diffraction pattern of area shown in Fig. 4a, containing an $[001]_{\gamma}$ zone and an $[012]_{M_6C}$ zone.
- Fig. 5. Microhardness of rapidly solidified and solid-state quenched Fe-W-C alloys as a function of tungsten content.
- Fig. 6. The microstructure of rapidly solidified T1 high speed tool steel, showing δ -ferrite cells surrounded by austenite and M_6C carbide.
- Fig. 7. Microhardness as a function of tempering time at 600°C for rapidly solidified and solid-state quenched FeWC1 (6.3wt%W).
- Fig. 8. Rapidly solidified FeWC1, tempered at 600°C for 40 minutes. Cementite has precipitated within the laths.

- Fig. 9a. SEM micrograph for rapidly solidified FeWC1, tempered at 600°C for 10 hours.
- Fig. 9b. STEM micrograph of rapidly solidified FeWC1, tempered at 600°C for 10 hours.
- Fig. 10. Microhardness as a function of tempering temperature for rapidly solidified and solid-state quenched FeWC6 alloy and T1 high speed tool steel.
- Fig. 11. Rapidly solidified FeWC6 (23wt%W) tempered at 650°C for 1 hour. M_6C precipitation has occurred within the δ -ferrite cells.
- Fig. 12. Rapidly solidified T1 high speed tool steel tempered at 615°C for 1 hour. A fine precipitation of M_2C carbide has occurred within the δ -ferrite cells.
- Fig. 13. The transformation temperatures as a function of composition in rapidly solidified iron-tungsten-carbon alloys.

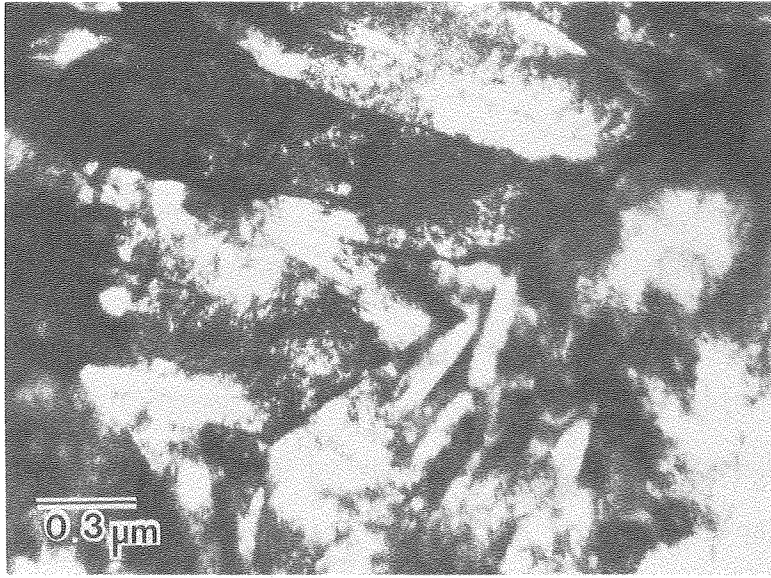


Fig. 1

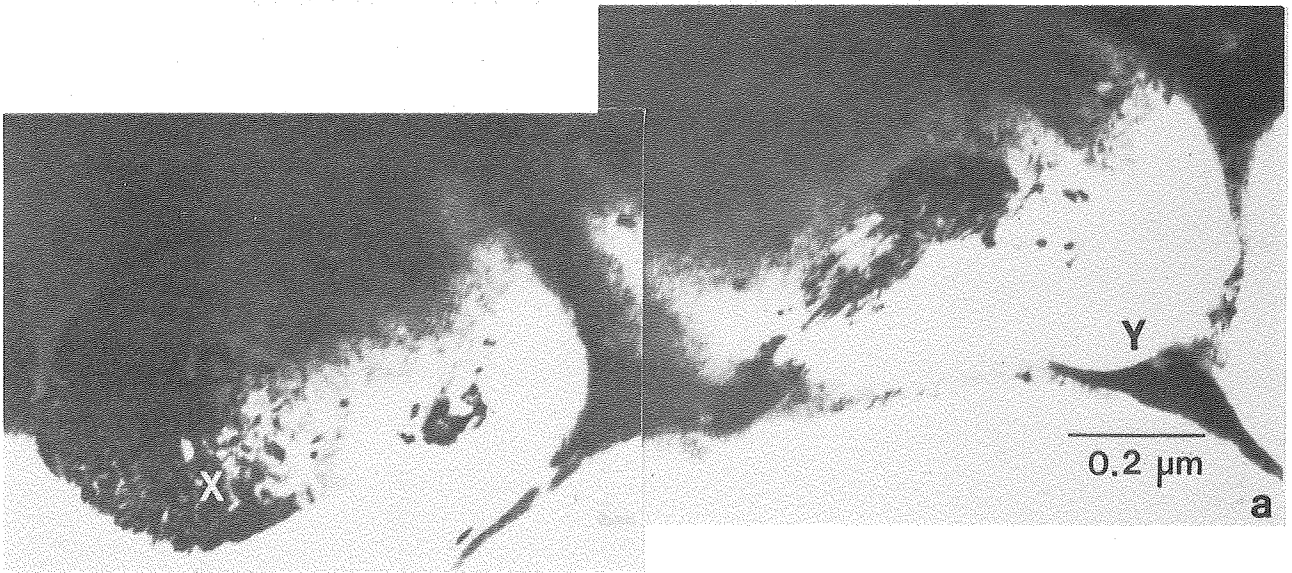


Fig. 2a

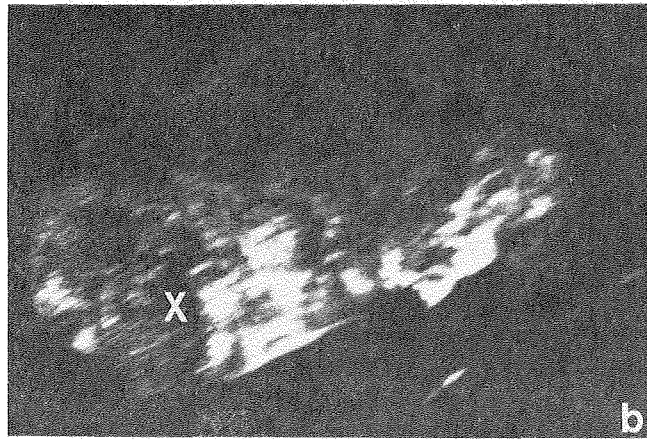


Fig. 2b



Fig. 2c

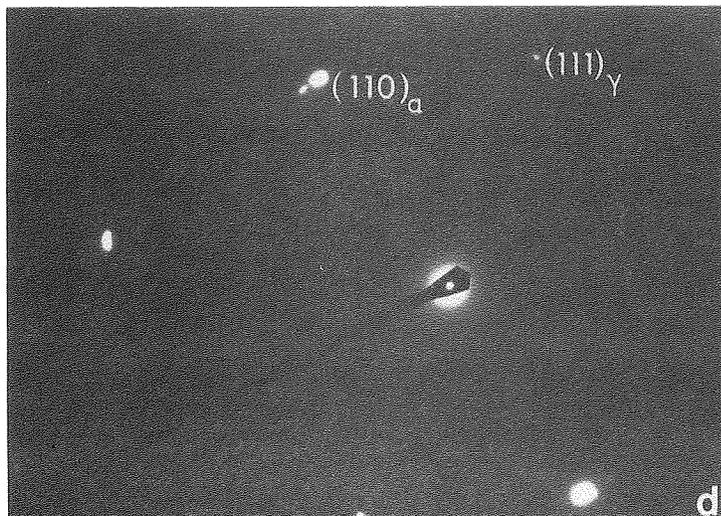


Fig. 2d

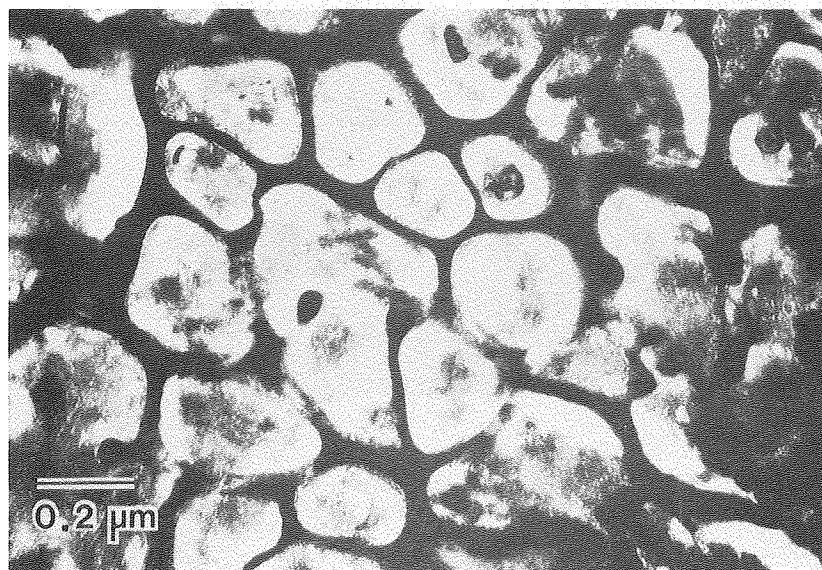


Fig. 3

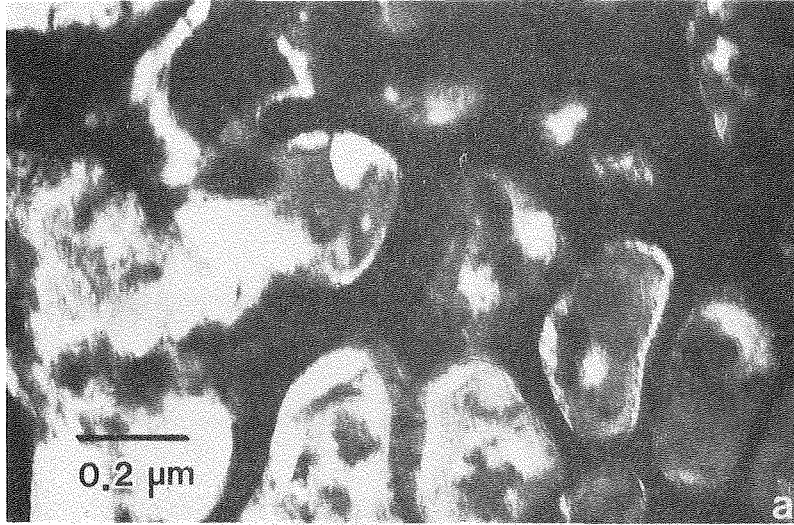


Fig. 4a

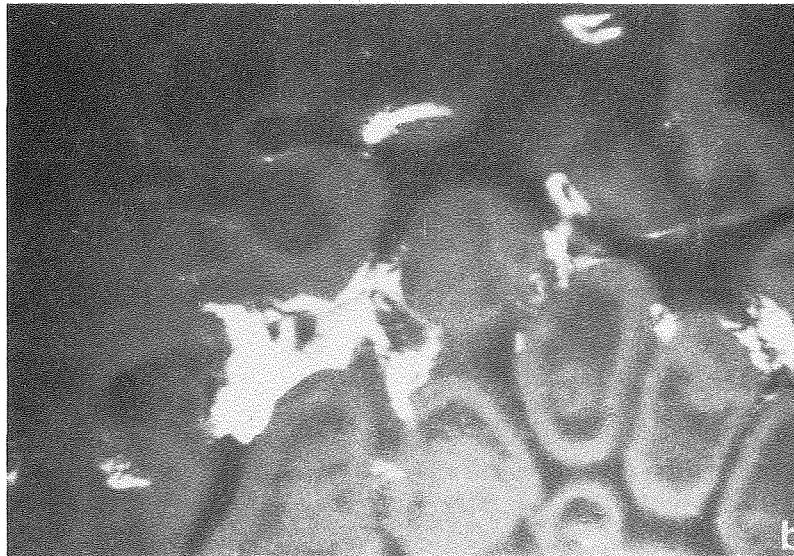


Fig. 4b

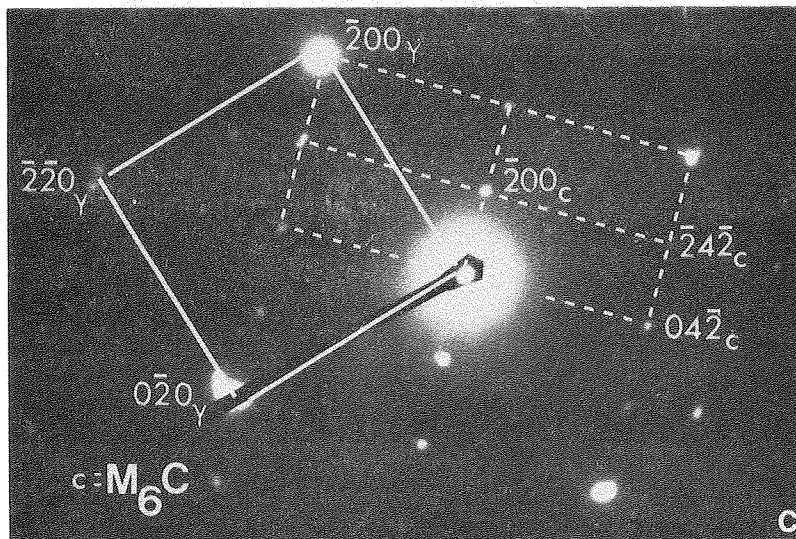


Fig. 4c

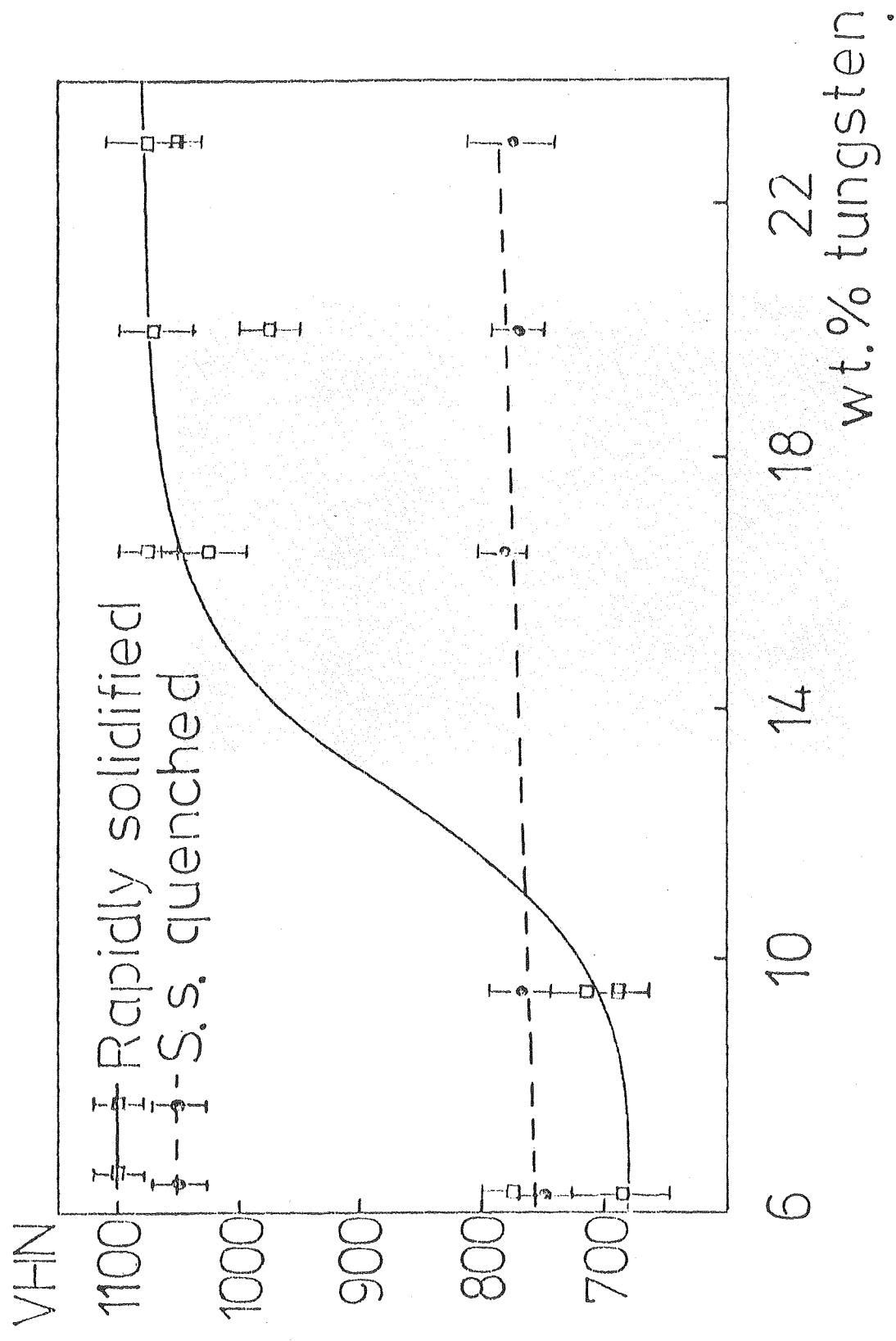


Fig. 5

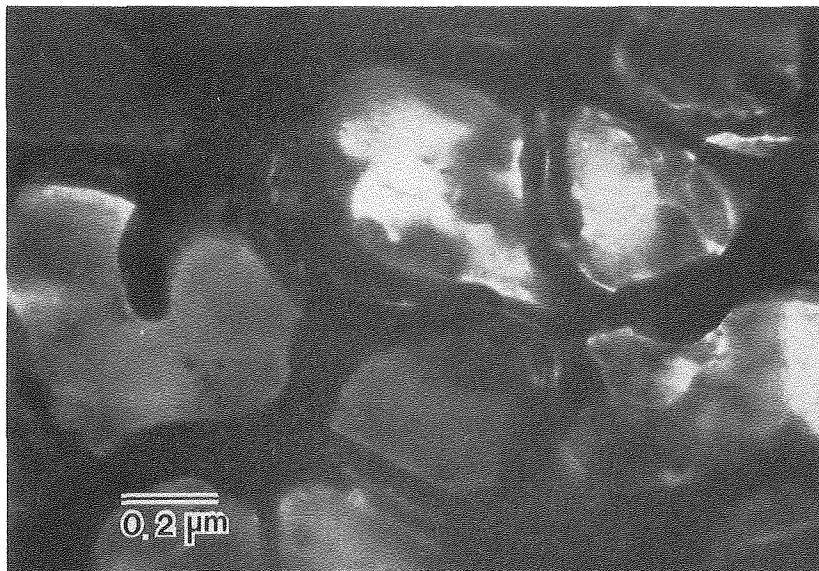


Fig. 6

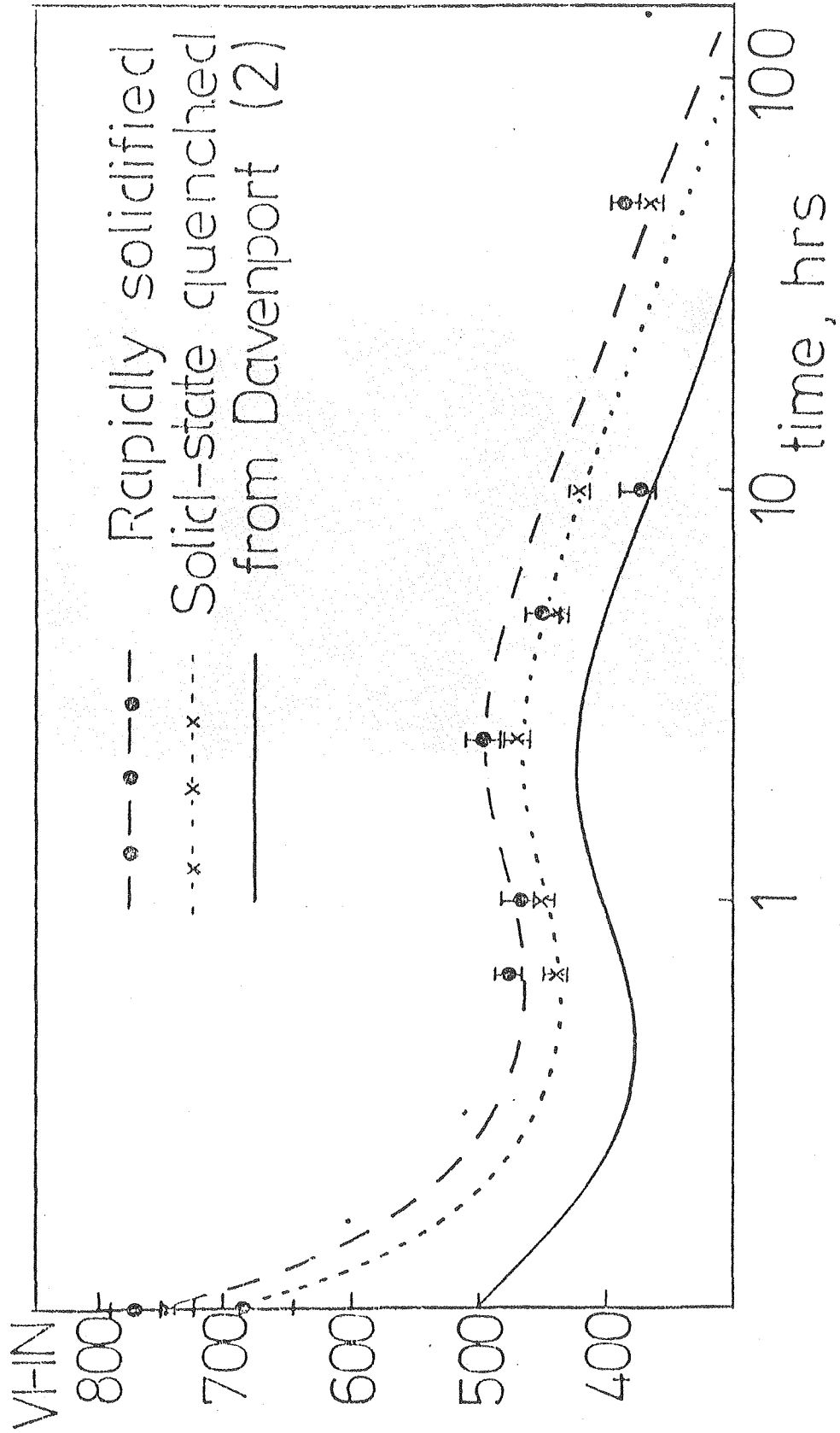


Fig. 7

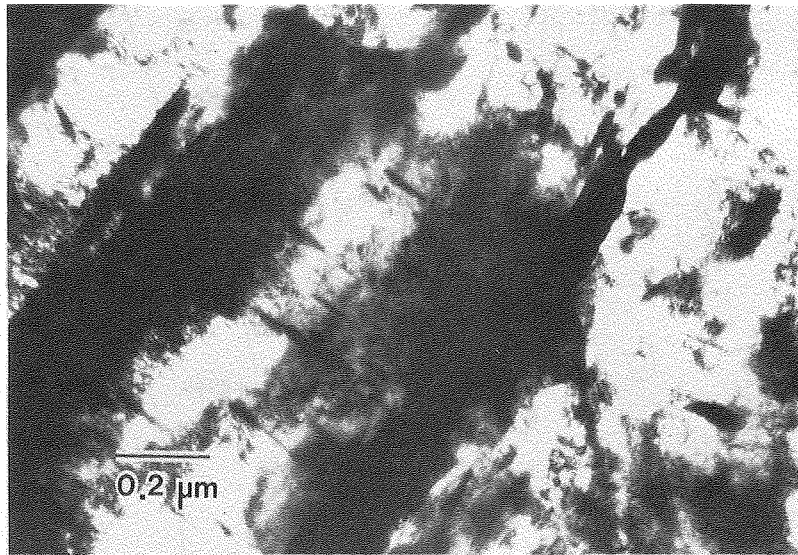


Fig. 8

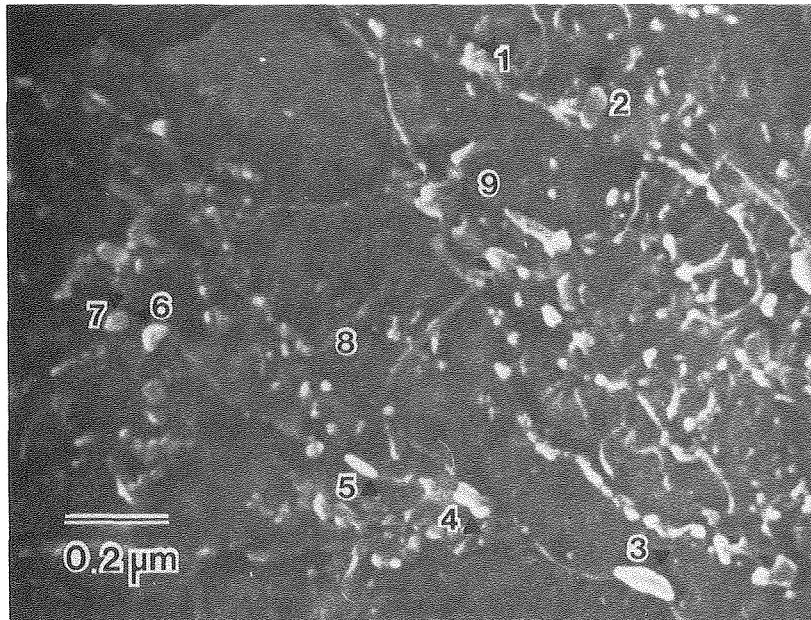


Fig. 9a

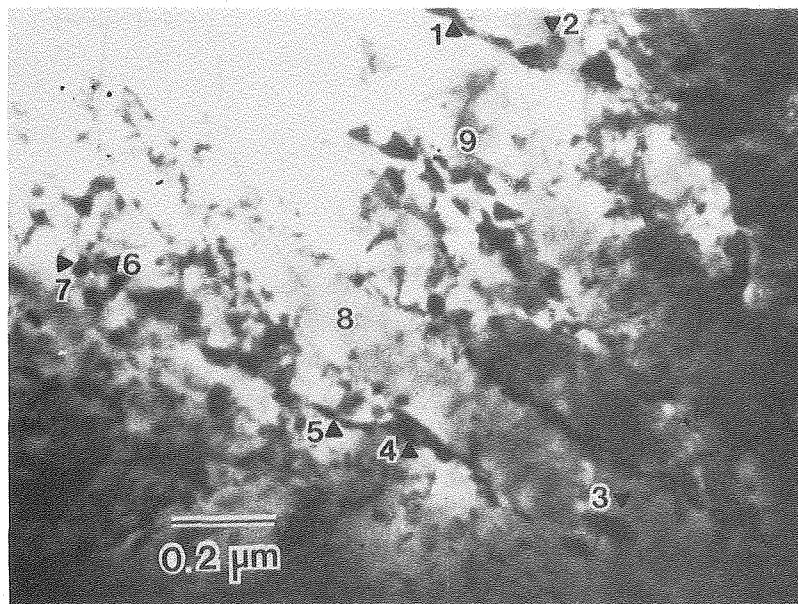


Fig. 9b

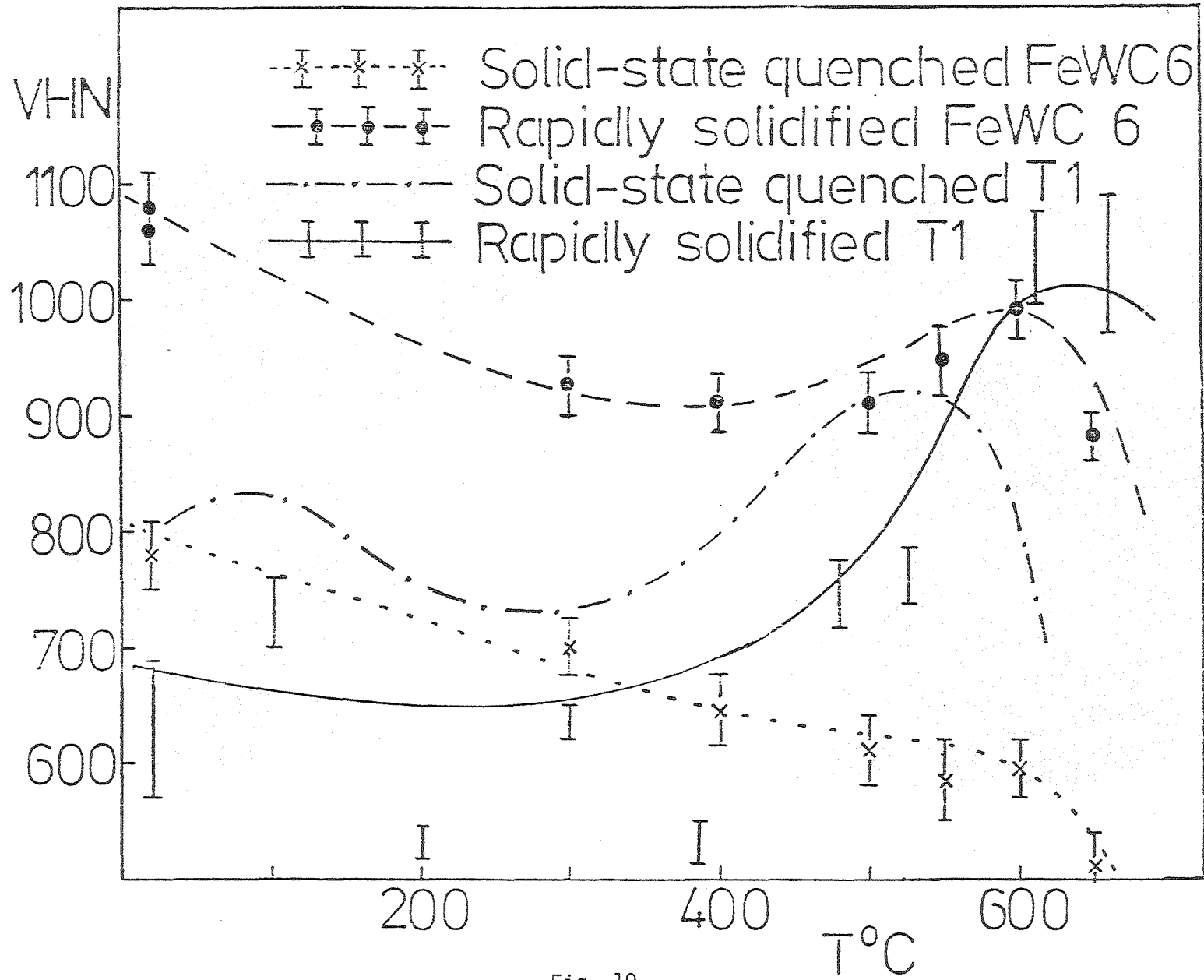


Fig. 10

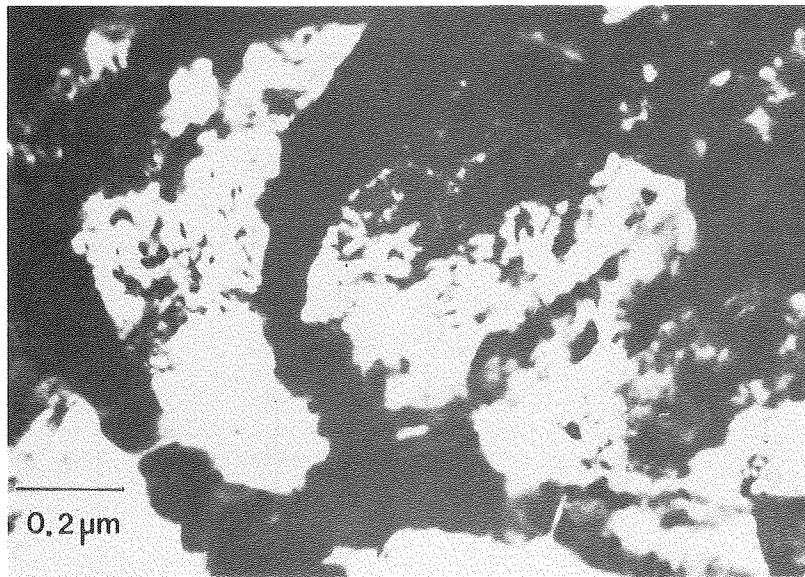


Fig. 11

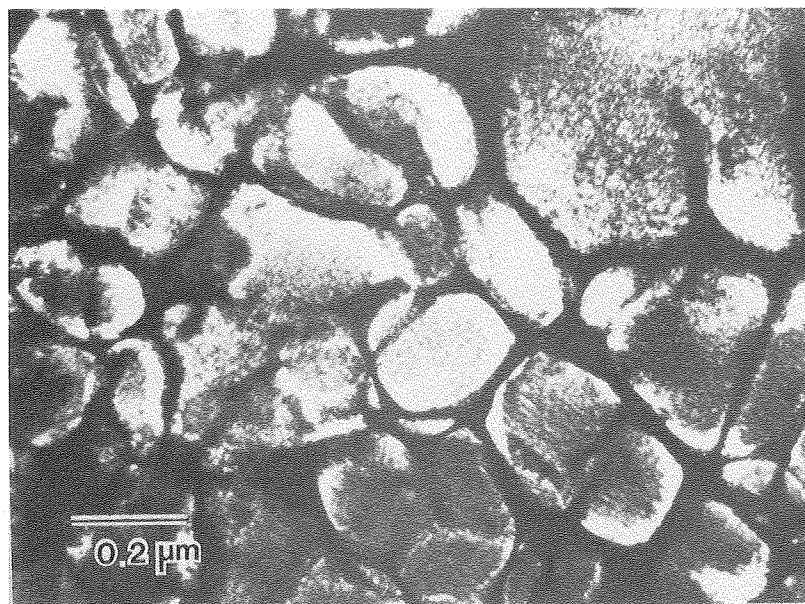


Fig. 12

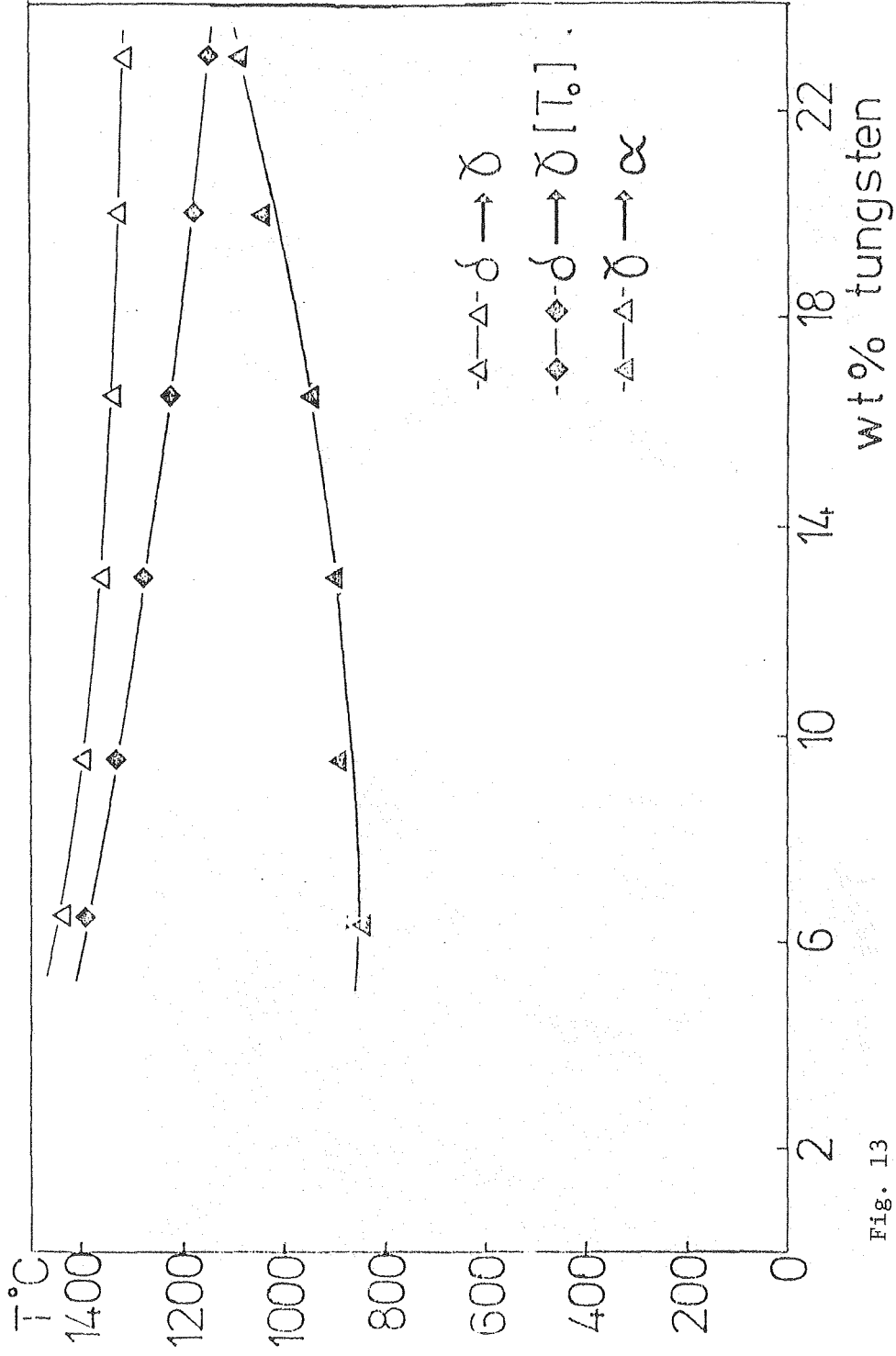


Fig. 13